Published online 5 April 2010 *Nucleic Acids Research, 2010, Vol. 38, No. 14* ***4821–4833***
doi:10.1093/nar/gkq219

DNA-binding properties of T4 UvsY recombination mediator protein: polynucleotide wrapping promotes high-affinity binding to single-stranded DNA

Hang Xu, Hans T. H. Beernink and Scott W. Morrical*

Department of Biochemistry, Department of Microbiology and Molecular Genetics, and Vermont Cancer Center, University of Vermont College of Medicine, Burlington, VT 05405, USA

Received February 12, 2010; Revised March 15, 2010; Accepted March 16, 2010

ABSTRACT

To carry out homologous recombination events in the cell, recombination proteins must be able to recognize and form presynaptic filaments on single-stranded DNA (ssDNA) in the presence of a vast excess of double-stranded DNA (dsDNA). Therefore recombination machineries stringently discriminate between ssDNA and dsDNA lattices. Recent single-molecule studies of bacteriophage T4 recombination proteins revealed that, surprisingly, the UvsY recombination mediator protein binds stronger to stretched dsDNA molecules than to stretched ssDNA. Here, we show that for relaxed DNA lattices, the opposite is true: UvsY exhibits a 1000-fold intrinsic affinity preference for ssDNA over dsDNA at moderate salt concentrations. This finding suggests that UvsY preferentially loads UvsX recombinase onto ssDNA under physiological conditions. The biochemical basis for high-affinity UvsY–ssDNA binding was investigated by hydrodynamic and cross-linking methods. Results show that UvsY forms ring-like hexamers in solution, and that ssDNA binds to multiple subunits within each hexamer, consistent with ssDNA wrapping. The data support a model in which ssDNA wrapping by UvsY protein is important for the selective nucleation of presynaptic filaments on ssDNA versus dsDNA, and for the coordinated transfer of ssDNA from Gp32 (SSB) to UvsY (RMP) to UvsX (recombinase) during filament assembly.

INTRODUCTION

Recombinases of the RecA/Rad51 family play central roles in homologous recombination and homology-directed DNA repair (1,2). RecA/Rad51 enzymes catalyze strand exchanges between homologous single-stranded DNA (ssDNA) and double-stranded DNA (dsDNA) molecules. A prerequisite for DNA strand exchange is the assembly of a presynaptic filament consisting of many molecules of recombinase bound cooperatively to ssDNA (3,4). The proper assembly of presynaptic filaments is crucial for maintaining genetic stability, as evidenced by defects in this process leading to hereditary cancer predisposition syndromes in humans (5,6).

Presynaptic filament assembly faces several biochemical hurdles in the cell: first, the ssDNA target for filament assembly is present only transiently (i.e. as a resected double-strand break or daughter-strand gap) and in vast deficit with respect to cellular dsDNA. Binding of dsDNA in the proper kinetic order following presynaptic filament assembly is an essential component of strand exchange. Inappropriate dsDNA binding during presynapsis is known to inhibit strand exchange (7–9). Second, the ssDNA target for filament assembly is sequestered by ssDNA-binding proteins (SSBs) that compete with recombinases for binding sites (10). Therefore the presynaptic filament assembly machinery must discriminate stringently between ssDNA and dsDNA lattices and also must successfully promote recombinase/SSB exchange on ssDNA.

Studies of the bacteriophage T4 recombination system have revealed many important biochemical principles involved in presynaptic filament assembly (10–12). The T4 recombination mediator protein, UvsY, has emerged as a central player in this system, along with UvsX

*To whom correspondence should be addressed. Tel: +1 802 656 8260; Fax: +1 802 656 8220; Email: smorrica@uvm.edu
Present addresses:
Hang Xu, Institute of Biophysics, Chinese Academy of Science, 15 Datun Road, Beijing 100101, People's Republic of China.
Hans T.H. Beernink, BioSource International, 542 Flynn Road, Camarillo, CA 93012, USA.

recombinase and Gp32, the T4 SSB protein. *In vitro*, UvsY stimulates the enzymatic activities of UvsX recombinase by promoting UvsX–ssDNA filament assembly, and by helping UvsX to displace bound Gp32 from ssDNA (10,13). UvsY is essential for UvsX catalytic activities at salt and Gp32 concentrations that simulate physiological conditions (13–18). *In vivo*, *uvsY* and *uvsX* mutants have equivalent recombination-deficient phenotypes, indicating that UvsX recombinase is dependent on UvsY for biological activity (19–21).

The biochemical properties of UvsY include binding to ssDNA and dsDNA, heteroprotein interactions with UvsX, Gp32 and Gp46/47 (T4 recombination nuclease), and self-association (11,14–16,22,23). Etheno-DNA-binding assays demonstrated that UvsY binds to ssDNA non-cooperatively but with high affinity, and with a binding site size of 4 nt residues per monomer (23). UvsY exists in solution predominantly as a 95 kDa hexamer, and binds to ssDNA in this form (22). Key features of UvsY's RMP activity include its ability to destabilize Gp32–ssDNA interactions and to stabilize UvsX–ssDNA interactions (16–18,24). The destabilization of Gp32–ssDNA interactions by UvsY is independent of UvsY–Gp32 protein–protein interactions (17,24), indicating that ssDNA structural changes induced by UvsY are responsible for the destabilization effect. UvsY can also directly displace Gp32 from ssDNA at low salt concentrations (24). UvsY–ssDNA interactions also play a major role in the observed stabilization of UvsX–ssDNA interactions (18,25).

UvsY also binds to dsDNA (14,24), and so must discriminate between ssDNA and dsDNA lattices in order to promote presynaptic filament assembly. Pant *et al*. (24) used force spectroscopy methods to measure the interactions of UvsY with single, stretched dsDNA molecules. The data showed that at high stretching forces, UvsY exhibits higher affinity for dsDNA than it does for ssDNA, a result that at first seems contrary to the need for presynaptic filament assembly on ssDNA. However, the same study showed that at low stretching forces, UvsY strongly wraps ssDNA created by exposure of stretched dsDNA to glyoxal (24). Together, these findings suggested that inter-conversions between extended and wrapped conformations of ssDNA could be important for UvsY-mediated trafficking of UvsX and Gp32 proteins on ssDNA. Similar inter-conversions could also be important for ssDNA/dsDNA discrimination by UvsY during presynapsis. However, the single-molecule studies of Pant *et al*. (24) were conducted under the highly artificial conditions of over-stretched dsDNA and/or ssDNA stabilized by chemical modification. Therefore it is important to establish the relationships between UvsY–ssDNA and UvsY–dsDNA interactions under native DNA conditions.

In this study, we measured and compared the intrinsic affinities of UvsY for relaxed, native ssDNA and dsDNA molecules at low binding density over a range of salt concentrations. The results indicate that individual UvsY hexamers strongly prefer binding to ssDNA over dsDNA under native DNA conditions and at physiologically relevant ionic strengths, which is opposite of what was observed in DNA stretching studies (24). This preference for ssDNA over dsDNA is preserved in UvsY mutants that greatly reduce its overall DNA-binding affinity. Results of sedimentation and cross-linking experiments indicate that UvsY forms ring-like hexamers in solution, and that ssDNA binds to multiple subunits within each hexamer, consistent with ssDNA wrapping. The data support a model in which ssDNA wrapping promotes the selective localization of UvsY on ssDNA, where it may direct the assembly of productive presynaptic filaments. Our studies of UvsY—native DNA interactions in the ensemble, combined with DNA stretching and mutagenesis data (24,25), support a mechanism of presynapsis in which UvsY captures an extended ssDNA conformation created by Gp32 and converts it into a wrapped conformation suitable for hand-off to UvsX recombinase. The coordinated hand-off of ssDNA from SSB to mediator to recombinase is likely to be a conserved mechanism in diverse recombination systems.

MATERIALS AND METHODS

Reagents, buffers and resins

All chemicals used were reagent grade and aqueous solutions were made with water purified through a Barnstead system. Buffer A used in quantitative DNA–cellulose chromatography experiments with UvsY and its mutants contained 20 mM Tris–HCl (pH 7.4) and variable concentrations of NaCl. Buffer B used in analytical ultracentrifugation experiments contained 20 mM Tris–HCl (pH 7.4), 1 mM $MgCl_2$ and variable concentrations of NaCl. ssDNA– and dsDNA–cellulose resins were prepared from salmon sperm DNA (Sigma) and Whatman CF-11 cellulose fibers as described (26). Two different batches of ssDNA–cellulose used in these studies contained 1.7 and 2.0 mg of total immobilized DNA per packed milliliter of resin, respectively, as determined by the release of A_{260} units upon boiling (26). By the same method, two different batches of dsDNA–cellulose used in these studies were shown to contain 0.6 and 1.0 mg, respectively, of total immobilized DNA per packed milliliter of resin.

Proteins and nucleic acids

Purification and storage conditions for T4 UvsY, $UvsY_{K58A}$ and $UvsY_{K58A,R60A}$ proteins were as described previously (23,27). The purity of each protein stock was >98% based on SDS–PAGE gels stained with Coomassie brilliant blue. All protein stocks were determined to be nuclease-free according to published criteria (28). The concentrations of protein stocks were determined by the absorbance at 280 nm, using an extinction coefficient of $19\,180\,M^{-1}\,cm^{-1}$ for UvsY wild-type and mutant proteins (29). HPLC-purified oligonucleotides (dT_4, dT_8, dT_{24}, dT_{25}) were purchased from Operon Biotechnologies and quantified by the absorbance at 260 nm using molar extinction coefficients provided by the manufacturer. The dT_{24} oligonucleotide was 5′-end labeled with [^{32}P] using T4 polynucleotide kinase (New England Biolabs), and purified by ethanol precipitation.

Quantitative DNA–cellulose chromatography

The sequence non-specific, intrinsic DNA-binding affinities of UvsY wild-type and mutant proteins for native ssDNA and dsDNA lattices were determined using quantitative DNA–cellulose affinity chromatography (30). Experiments were carried out at very low binding densities of protein on nucleic acid, which allows direct measurements of intrinsic association constants independent of the binding site size and cooperativity parameters of the proteins (31). The ssDNA– and dsDNA–cellulose resins were packed into 2 ml columns and pre-equilibrated with 2 ml buffer A containing different fixed concentrations of NaCl at a flow rate of 40 ml/h. Hexamers (0.67 nmol) of either UvsY, $UvsY_{K58A}$ or $UvsY_{K58A,R60A}$ in 2 ml of the same buffer were loaded onto the columns by gravity (UvsY hexamers/total nucleotide residues molar ratio $\approx 10^{-4}$). The flow was then stopped and the loaded columns allowed to sit for 10–15 min, which was sufficient to achieve an initial binding equilibrium since doubling the loading time had no effect on results. Thereafter, 20 ml of the same buffer followed by 10 ml of buffer A plus 1 M NaCl was used to elute proteins from columns, with a flow rate of 40 ml/h while 1 ml fractions were collected. The protein concentration in each fraction was quantified by intrinsic tryptophan fluorescence (excitation wavelength: 295 nm; emission wavelength: 340 nm) on a Quantamaster QM6 fluorometer (Photon Technology International, South Brunswick, NJ). To obtain the best signal/noise ratio, the excitation/emission bandpass was set at 2 nm/3 nm. Fluorescence data points represented an average of 20 fluorometer readings and were compared to calibration curves to obtain protein concentrations. All chromatography steps and fluorescence measurements were carried out at room temperature (typically 23°C).

Chromatography elution profiles are presented in the following format (30,31): $\log P_{ci}$ versus fraction number, in which P_{ci} denotes the percentage of protein remaining on columns and is calculated by the protein quantity in each fraction and the total protein quantity. This type of plot typically yields a linear relation of data points and the slope is equal to $-\log(1+k)$, in which k is a proportionality constant. After obtaining this proportionality constant for each data set, the association constant of protein to DNA at a given NaCl concentration was calculated according to the following equation:

$$K = \frac{V_f}{kD_t} \quad (1)$$

where K is the intrinsic association constant of protein to DNA; V_f is the fraction volume; and D_t is the total molar amount of protein-accessible DNA on the column, which was determined as follows (30,31): the 2 ml column resin was taken out and resuspended in 10 ml of DNaseI-cleavage buffer containing 20 mM Tris (pH 7.4), 10 mM $MgCl_2$ and 100 mM NaCl. DNaseI (2 mg) was then added to this mixture and incubated at 37°C for 4 h. The nucleotides released into solution were considered protein-accessible and determined by phosphate analysis as described (32). Briefly, 10 µl of sample solution was mixed with 30 µl of $Mg(NO_3)_2$ (10% dissolved in 95% ethanol) and ashed over flame. HCl (0.5N, 0.3 ml) was then added to hydrolyze pyrophosphate formed in the last step. After hydrolysis at 100°C for 15 min, 0.6 ml of ammonium molybdate (0.42% dissolved in 1 N H_2SO_4) and 0.1 ml of 10% ascorbic acid were mixed with the sample and incubated at 45°C for 20 min. Absorbance at 820 nm was then measured and converted to the quantity of nucleotide using a conversion factor of 0.260 absorbance unit = 0.01 µmol of nucleotides. The total amounts of protein-accessible DNA in ssDNA– and dsDNA–cellulose columns were determined to be 7.2 ± 0.5 µmol and 2.3 ± 0.2 µmol of nucleotide residues, respectively. Thus the binding density of UvsY hexamers per protein-accessible nucleotide residue was $\leq 3 \times 10^{-4}$ in all experiments.

Analytical ultracentrifugation

Sedimentation equilibrium and velocity studies were carried out as previously described (22). All experiments were performed in a Beckman Optima XL-I analytical ultracentrifuge (Beckman Coulter Inc., Fullerton, CA) equipped with both absorbance and Rayleigh interference optics. All experiments utilized a Beckman An50-Ti 8-hole rotor equipped with either two- or six-sector charcoal-filled epon centerpieces and sapphire windows. The rotor temperature was set between 20 and 25°C depending on the experiment. Buffers consisted of buffer B plus variable concentrations of NaCl. All solutions were sterile filtered prior to use.

The stoichiometry of UvsY-oligonucleotide complexes was evaluated in solution using a modification of the meniscus depletion sedimentation equilibrium method (33). Specific rotor conditions are selected that quantitatively remove the desired solute from the radial position immediately adjacent to the solution–air meniscus. For the case of hexameric UvsY protein, meniscus depletion is achieved at equilibrium after 17 h at 18 000 rpm, 22°C, in buffer B plus 300 mM NaCl, using a solution column height of ~3.5 mm. Solutions containing both protein and oligonucleotide ssDNA were subjected to meniscus depletion sedimentation until equilibrium was achieved. In all cases, oligonucleotide ssDNA (dT_4, dT_8 or dT_{25}; 75 µM nucleotide residues) was present in large stoichiometric excess over UvsY (4.5 µM monomers) assuming a binding site size of $n = 4$ nucleotide residues/monomer (23). Control experiments were identical except that buffer contained 500 mM NaCl and lower concentrations of solutes (25 µM oligonucleotides and 1.5 µM UvsY). Evaluation of the state of equilibrium was performed as previously described (22). Radial absorbance measurements were collected at two wavelengths (260 and 280 nm) within a narrow radial interval corresponding to the meniscus depleted region. As the molecular weight of the UvsY hexamer ($M_r \approx 95\,000$) is very much greater than the largest oligonucleotide used in these studies (dT_{25}, $M_r \approx 7500$), only the protein-containing species are able to achieve meniscus depletion. Because of this, the only observable absorbance within a narrow range immediately adjacent to the solution–air meniscus must

result from absorbance due to free ssDNA species residing in the otherwise depleted region. This assumption is reasonable since sedimentation velocity data indicate that the UvsY hexamer is non-dissociable under identical conditions, either by itself or when bound to ssDNA (22). Therefore the UvsY hexamer represents the *smallest* protein species available in this controlled system.

Hydrodynamic modeling

Hydrodynamic modeling was performed using directly measured sedimentation and frictional coefficients (s and f, respectively) for all species (22). All hydrodynamic parameters were corrected to 20°C and zero concentration of sedimenting solute in water (34). Molecular masses of protein and nucleoprotein complexes were calculated from primary sequence data for UvsY (35) and oligonucleotides (Operon Technologies). The partial specific volume, $\bar{\nu}$, of the UvsY–ssDNA complex was calculated using a $\bar{\nu}$ estimate for ssDNA of 0.55 cm^3/g (T. Laue, personal communication) and weight-averaging the contribution of both components in the complex. This method makes the assumption that the $\bar{\nu}$ of each component does not change upon association. Theoretical frictional coefficients, f_0, were calculated as described, using volumetric determinants obtained from macromolecular crystallography data (34,36). Calculation of f_0 depends on R_p, the 'equivalent radius', which is the expected radius of a rigid, impermeable and incompressible sphere having the identical volume as the species of interest. R_p and f_0 values were calculated from Equations (2) and (3), respectively:

$$R_p = 6.72 \times 10^{-9} M_r^{1/3} \quad (2)$$

$$f_0 = 6\pi n R_p \quad (3)$$

where η is the viscosity parameter. Note that f_0 calculated in this manner corresponds to the predicted *minimum* value of the frictional coefficient, and therefore results in a *maximum* estimation of the sedimentation coefficient, s, according to the Svedberg relationship:

$$s = \frac{M(1 - \bar{\nu}\rho)}{N_0 f} \quad (4)$$

where ρ equals density and N_0 is Avogadro's number. The value of f/f_0 gives a rough approximation of the asymmetry of the solute species, indicating the deviation from an ideal sphere.

Structural models of associated oligomers were calculated using hydrodynamic simulation and the relationship between predicted sedimentation parameters of monomers and their oligomeric assemblies (37–40). Here the monomeric sedimentation coefficient is related to the n-state of oligomeric assembly by Equations (5) and (6):

$$s_n^0 = \left[1 + \frac{1}{n} \sum_i^n \sum_j^n \frac{1}{\alpha_{ij}}\right] s_1^0 \quad (5)$$

where

$$\alpha_{ij} = \frac{R_{ij}}{R_0} \quad (6)$$

In this relationship, s_n^0 is the sedimentation coefficient predicted for a rigid structure containing n identical spherical units, each with radius R_0 and sedimentation coefficient s_1^0. R_{ij} is the radial distance between units, and therefore α_{ij} is determined by the assumed geometry of unit assembly. By designing various models that describe a state of n-assembly, theoretical sedimentation parameters can be determined.

Photochemical crosslinking of UvsY-dT_{24}

5′-[^{32}P]-labeled dT_{24} (2 μM nucleotides) was incubated with or without 0.5 μM UvsY at ambient temperature, in buffer A plus 300 mM NaCl for 30 min to achieve equilibrium. The above reaction solutions (20 μl) were spotted onto a paraffin wax sheet (ParaFilm) and subjected to UV exposure for the indicated times. UV light (254 nm) was applied maintaining ~1 cm between the liquid drop and the UV source (hand-held UV lamp, UVP Inc.). After UV crosslinking, samples were brought to 0.02% SDS and heated to 100°C to fully disrupt non-covalent structures. Crosslinked species were separated by SDS–PAGE and visualized by autoradiography.

RESULTS

Intrinsic affinity of UvsY protein for isolated sites on DNA

To establish the relationships between UvsY–ssDNA and UvsY–dsDNA interactions under native DNA conditions, we measured the binding of UvsY to isolated sites on relaxed, unmodified dsDNA and ssDNA molecules, using the quantitative DNA–cellulose chromatography method (30,31). Measurements were made at very low binding densities of protein on DNA ($\leq 3 \times 10^{-4}$ UvsY hexamers per protein-accessible nucleotide residue; see 'Materials and Methods' section). For proteins that bind to DNA with a cooperativity parameter ω, binding to isolated sites is observed when the binding density $\nu \leq 1/10\omega$ (31). UvsY binds non-cooperatively to ssDNA ($\omega \approx 1$) (23). Therefore the experimental conditions are consistent with UvsY binding to isolated, not contiguous sites on DNA, and the binding constants measured are intrinsic affinity values that do not depend on cooperativity or binding site size (31). The intrinsic affinity parameters of UvsY–dsDNA and UvsY–ssDNA interactions were measured as functions of salt. These studies provide the first quantitative details of UvsY–dsDNA and UvsY–ssDNA interactions under native DNA conditions, and allow direct comparisons of both under identical solution conditions.

The elution profiles of UvsY from dsDNA–cellulose and from ssDNA–cellulose are shown in Figure 1A and B, respectively, and the derived intrinsic association constants (K_{ds} and K_{ss} values) are listed in Table 1. The results demonstrate that UvsY binds to dsDNA strongly

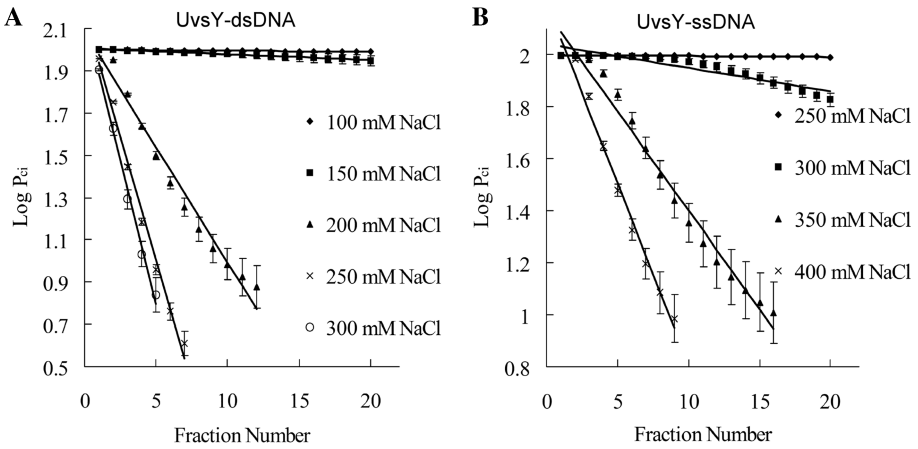

Figure 1. Salt-dependent elution of UvsY protein from dsDNA– and ssDNA–cellulose columns. Elution profiles are presented in the format of Log P_{ci} versus fraction number as described in 'Materials and Methods' section. UvsY (4 nmol) was loaded onto and eluted from dsDNA–cellulose columns (**A**) or ssDNA–cellulose columns (**B**) in buffer A plus various concentrations of NaCl as denoted in the figure. The fractions were quantified by intrinsic tryptophan fluorescence (excitation 295 nm, emission 340 nm) and calibrated against known concentrations of UvsY. All data points are averaged values from three independent experiments and standard deviations are shown as error bars. At low NaCl concentrations, the error bars are too small to be visualized on the plots.

Table 1. Intrinsic association constants of wild-type and mutant UvsY proteins for dsDNA and ssDNA lattices[a]

[NaCl] (mM)	UvsY		$UvsY_{K58A}$		$UvsY_{K58A,\ R60A}$	
	K_{ds} (M^{-1})	K_{ss} (M^{-1})	K_{ds} (M^{-1})	K_{ss} (M^{-1})	K_{ds} (M^{-1})	K_{ss} (M^{-1})
50	*4.0×10^{7}*[b]	N.D.	$1.1 \pm 0.03 \times 10^{3}$	$1.5 \pm 0.2 \times 10^{4}$	$2.8 \pm 0.01 \times 10^{2}$	$2.9 \pm 0.2 \times 10^{3}$
100	$3.5 \pm 1.1 \times 10^{5}$	N.D.	N.D.	$6.2 \pm 0.4 \times 10^{3}$	N.D.	N.D.
150	$7.1 \pm 1.7 \times 10^{4}$	N.D.	N.D.	$2.0 \pm 0.1 \times 10^{3}$	N.D.	N.D.
200	$1.5 \pm 0.1 \times 10^{3}$	*3.8×10^{6}*[b]	N.D.	$1.5 \pm 0.1 \times 10^{3}$	N.D.	N.D.
250	$6.1 \pm 0.7 \times 10^{2}$	$1.8 \pm 1.0 \times 10^{5}$	N.D.	*1.0×10^{3}*[b]	N.D.	N.D.
300	$5.0 \pm 0.5 \times 10^{2}$	$2.1 \pm 1.0 \times 10^{4}$	N.D.	N.D.	N.D.	N.D.
350	N.D.	$7.3 \pm 1.0 \times 10^{2}$	N.D.	N.D.	N.D.	N.D.
400	N.D.	$3.7 \pm 0.4 \times 10^{2}$	N.D.	N.D.	N.D.	N.D.

N.D., not determined.
[a]K_{ds} and K_{ss} equal intrinsic association constants of UvsY or mutants for dsDNA and ssDNA, respectively, measured at the indicated NaCl concentrations. Numbers in plain text represent the averages ± standard deviation from three independent quantitative DNA–cellulose experiments similar to those shown in Figures 1–3. The reaction conditions were as described in 'Materials and Methods' section and in the text.
[b]Numbers in italics represent projected K_{ds} and K_{ss} values derived from plots in Figure 4 by extrapolation.

under relatively low-salt conditions ($K_{ds} \approx 10^{5}$–$10^{7}\ M^{-1}$ in 50–100 mM NaCl), however UvsY–dsDNA binding affinity decreases dramatically with increasing salt concentration, becoming quite weak at 200 mM NaCl and undetectable by this method above 300 mM NaCl (Figure 1A, Table 1).

UvsY exhibits much higher intrinsic affinities for ssDNA than for dsDNA when measured by the DNA-cellulose method (Figure 1B, Table 1). At 250 mM NaCl, the ratio of directly measured association constants $K_{ss}/K_{ds} \approx 300$, while at 200 mM NaCl the projected $K_{ss}/K_{ds} \approx 2500$ (Table 1; see also Figure 4). NaCl (200 mM) is taken as a reasonable approximation of physiological ionic strength since the UvsY-dependence of UvsX biochemical activities at this salt concentration mimics the genetic requirement for both proteins in T4 recombination pathways (19–21). Therefore we conclude that the intrinsic affinity of UvsY for relaxed ssDNA exceeds that for relaxed dsDNA by at least three orders of magnitude at physiologically relevant ionic strengths. Intrinsic UvsY–ssDNA association constants at lower salt concentrations are too high to be measured by the DNA–cellulose method.

Missense mutations destabilize UvsY–DNA interactions

Missense $UvsY_{K58A}$ and double missense $UvsY_{K58A,R60A}$ mutant proteins have been characterized in our laboratory, and shown qualitatively to have decreased ssDNA-binding activity while retaining overall hexameric structure (18,27). To quantify their defects, the binding of both mutants to dsDNA– and ssDNA–cellulose columns was measured (Figures 2 and 3), and the derived intrinsic association constants are listed in Table 1. Figure 2A and B shows the elution profiles of $UvsY_{K58A}$ from dsDNA– and ssDNA–cellulose columns, respectively. Figure 3A

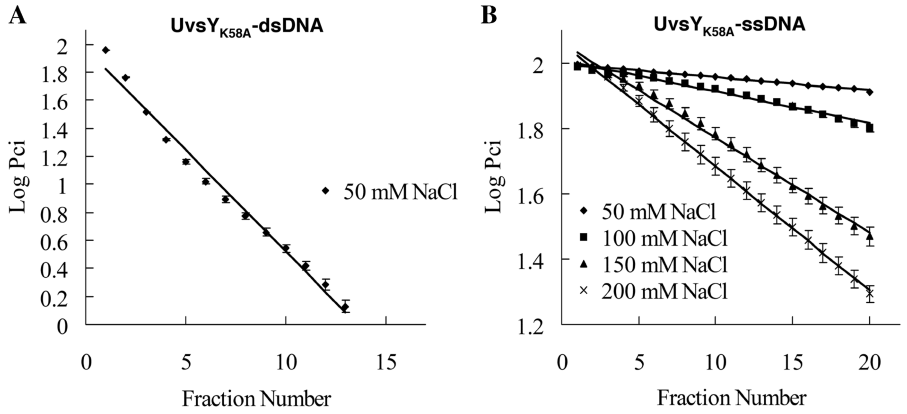

Figure 2. Salt-dependent elution of UvsY$_{K58A}$ single mutant protein from dsDNA– and ssDNA–cellulose columns. UvsY$_{K58A}$ (4 nmol) was loaded onto and eluted from dsDNA–cellulose columns (**A**) or ssDNA–cellulose columns (**B**) in buffer A plus various concentrations of NaCl as denoted in the figure. All other experimental details were identical to those reported in Figure 1.

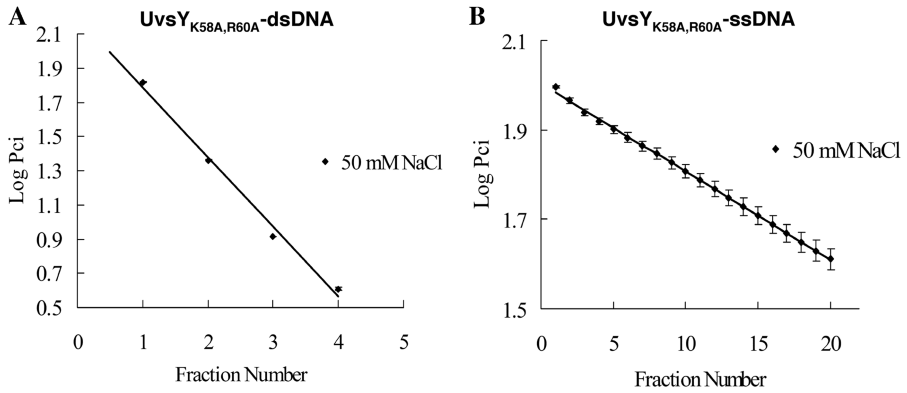

Figure 3. Salt-dependent elution of UvsY$_{K58A,R60A}$ double mutant protein from dsDNA– and ssDNA–cellulose columns. UvsY$_{K58A,R60A}$ (4 nmol) was loaded onto and eluted from dsDNA–cellulose columns (**A**) or ssDNA–cellulose columns (**B**) in buffer A plus various concentrations of NaCl as denoted in the figure. All other experimental details were identical to those reported in Figure 1.

and B shows the elution profiles of UvsY$_{K58A,R60A}$ from dsDNA– and ssDNA–cellulose columns, respectively. The intrinsic affinities of both UvsY mutants for both lattices are dramatically reduced compared to wild-type UvsY. K_{ds} values of both mutants can only be accurately determined at low salt (50 mM NaCl), and are at least 10^4-fold lower than wild-type (Table 1). UvsY$_{K58A}$ exhibits ~5-fold higher affinity for both ssDNA and dsDNA than does UvsY$_{K58A,R60A}$ in experiments performed at 50 mM NaCl. At the same salt concentration, the ratio $K_{ss}/K_{ds} \approx 14$ for UvsY$_{K58A}$ and ≈ 10 for UvsY$_{K58A,R60A}$. Therefore in both mutants, the intrinsic affinities for ssDNA are higher than those for dsDNA, which follows the same trend as wild-type UvsY. The UvsY$_{K58A}$ mutant exhibits detectable binding to ssDNA–cellulose at salt concentrations up to 200 mM NaCl, but its K_{ss} value is projected to be at least 10^3-fold lower than wild-type at 200 mM NaCl (Table 1; see also Figure 4). These observations are consistent with the weak binding of these mutants to etheno-modified ssDNA and to stretched dsDNA that was previously reported, and may explain their partial defects in stabilizing UvsX–ssDNA complexes and in stimulating UvsX enzymatic activities (13,18,24,27).

UvsY exhibits different electrostatic binding modes for ssDNA and dsDNA

Salt effects on K_{ss} and K_{ds} for UvsY–DNA interactions were determined from the slopes of plots of logK_{ss} or logK_{ds} versus log[NaCl] (Figure 4, Table 2). The slope dlog K/dlog[NaCl] is related to the number of ionic interactions involved in protein–DNA binding (41–44). The magnitude of dlog K_{ss}/dlog[NaCl] for UvsY–ssDNA interactions is very large, –13.9, indicative of highly electrostatic binding. In contrast, the magnitude of dlog K_{ss}/dlog[NaCl] for UvsY$_{K58A}$–ssDNA interactions is only –1.7, demonstrating a major disruption of electrostatic binding determinants caused by the loss of this single basic residue within each subunit of a UvsY hexamer (Figure 4, Table 2). Interestingly, the magnitude of dlog K_{ds}/dlog[NaCl] for UvsY–dsDNA interactions is –6.6 (Figure 4, Table 2), or approximately half that observed with the ssDNA lattice. Therefore UvsY exhibits different binding modes for ssDNA and dsDNA, involving large

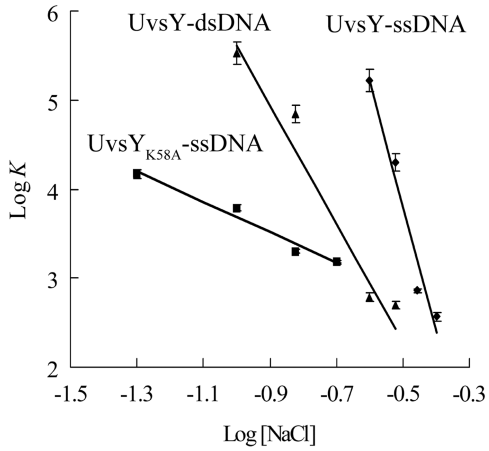

Figure 4. Ion effects on the intrinsic association constants of UvsY for ssDNA and dsDNA, and of $UvsY_{K58A}$ for ssDNA, respectively. The log–log plots are made using K_{ss} and K_{ds} values and corresponding NaCl concentrations listed in Table 1. The error bars represent the standard deviation from three independently determined K_{ss} or K_{ds} values for UvsY–ssDNA (diamonds), UvsY–dsDNA (triangles) and $UvsY_{K58A}$–ssDNA (squares) interactions. The data in each series have been fitted to a line yielding slopes representing the $d\log K_{(ss\ or\ ds)}/d\log[NaCl]$ values for UvsY–dsDNA, UvsY–ssDNA and $UvsY_{K58A}$–ssDNA interactions. These $d\log K_{(ss\ or\ ds)}/d\log[NaCl]$ values (slopes) are summarized in Table 2.

Table 2. Salt effects on the intrinsic association constants of UvsY–DNA interactions

UvsY protein	Lattice	$d\log K/d\log[NaCl]$[a]
Wild-type	dsDNA (ds)	−6.6
Wild-type	ssDNA (ss)	−13.9
K58A	ssDNA (ss)	−1.7

[a]Slopes derived from log–log plots of intrinsic association constant (K_{ss} or K_{ds}) versus [NaCl] as shown in Figure 4 and described in the text.

differences in the electrostatic component of binding. Implications for UvsY structure and function are discussed below (see 'Discussion' section).

ssDNA contacts multiple subunits within an UvsY hexamer

Previous sedimentation studies demonstrated that UvsY exists as a monodisperse hexamer of 95 kDa at salt concentrations ≥200 mM NaCl (22). The hexameric structure of UvsY protein suggests that it could wrap ssDNA around itself through contacts of multiple subunits with polynucleotide. To test this multi-subunit binding hypothesis, we performed meniscus depletion sedimentation equilibrium experiments to measure the stoichiometries of small oligonucleotides (dT_4, dT_8 and dT_{24}) bound to UvsY. Results of one such experiment are shown in Figure 5. In all cases, control experiments conducted at the non-permissive salt concentration of 500 mM NaCl resulted in no co-sedimentation of oligonucleotides with UvsY protein (Figure 5A), consistent

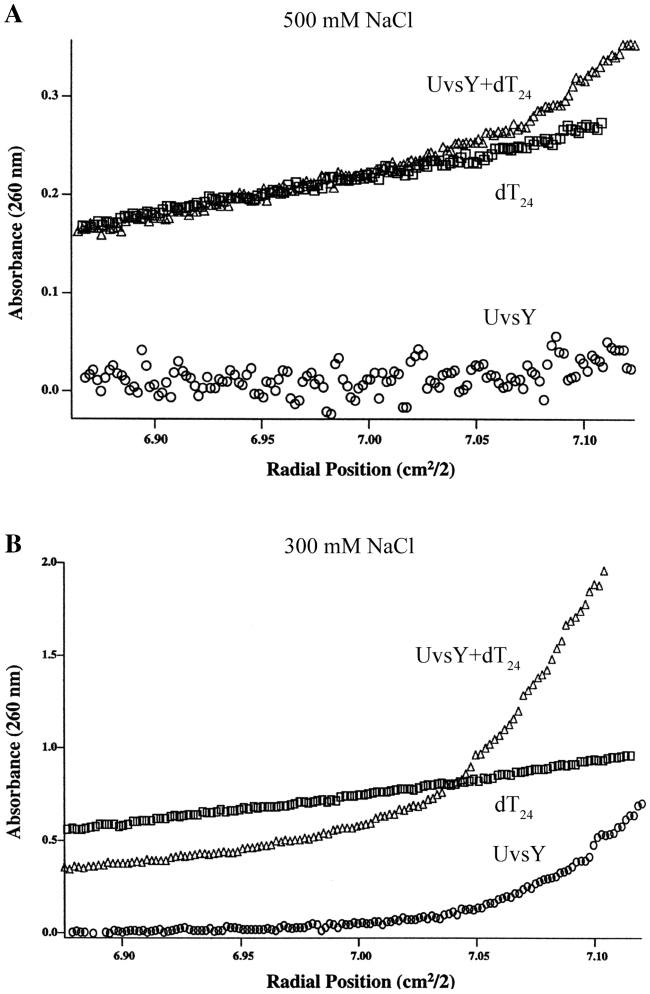

Figure 5. Meniscus depletion of dT_{24} oligonucleotide by UvsY protein. Meniscus depletion sedimentation equilibrium experiments were carried out as described in 'Materials and Methods' section. (**A**) Depletion experiments conducted under non-DNA-binding conditions (buffer B plus 500 mM NaCl) show no co-sedimentation of oligonucleotide dT_{24} with UvsY. (**B**) Similar experiments conducted under permissive conditions for DNA binding (buffer B plus 300 mM NaCl) show a ~1:1 stoichiometry of $UvsY_6$:dT_{24}. In both experiments, oligonucleotide dT_{24} alone (squares), UvsY alone (circle) or both (triangles) were centrifuged to equilibrium in a Beckman Optima XL-I analytical ultracentrifuge while scanning the absorbance at 260 and 280 nm. Co-sedimentation of dT_{24} with UvsY under permissive binding conditions lowers absorbance at the meniscus, allowing calculation of complex stoichiometry.

with previous results (22). In contrast, when experiments were performed at the permissive salt concentration of 300 mM NaCl, meniscus depletion of the oligonucleotide dT_{24} by co-sedimentation with UvsY was evident (Figure 5B). The loss of DNA absorbance at the meniscus allowed us to calculate a binding stoichiometry of 1.2 dT_{24} molecules per UvsY hexamer, a value consistent with previous measurements of 1:1 stoichiometric interactions between UvsY hexamers and dT_{24} or dT_{25} oligos [(22), H. Xu, H. Beernink and S. Morrical, unpublished results]. Similar meniscus depletion studies performed with dT_4 and dT_8 oligonucleotides in 300 mM

NaCl (data not shown) yielded stoichiometries of 5.3 and 2.7 oligos/hexamer, respectively. Given a solution average binding site size of $n = 4$ nt residues per UvsY monomer (23), the meniscus depletion data provide clear evidence that multiple subunits within the UvsY hexamer can interact with their binding sites on ssDNA simultaneously. The most dramatic example is given by the dT_4 oligo, which at 5.3 oligos/hexamer approaches the theoretical maximum of six oligos/hexamer. Therefore with a short enough oligo, it appears that all subunits of the UvsY hexamer retain the ability to interact with ssDNA.

The situation may be more complex with a longer oligo, however, as shown by the UV cross-linking experiment in Figure 6. Here, the specific salt concentration of 300 mM NaCl was chosen to allow formation of a discrete $UvsY_6$–dT_{24} complex (22). Therefore, the interaction between UvsY monomers and ssDNA was restricted to within the hexameric unit. 5′-[^{32}P]-labeled dT_{24} was incubated with UvsY and exposed to 254 nm UV light, then the crosslinked species were separated by SDS–PAGE and detected by autoradiography. The denaturing gel disrupts non-covalent interactions so that the [^{32}P]-labeled crosslinked species should consist of a single dT_{24} molecule plus any UvsY monomers that are crosslinked to it. As shown in Figure 6, the presence of multiple crosslinked species (lanes 4 and 6) indicates that multiple UvsY monomers within the hexamer can simultaneously contact the dT_{24} oligonucleotide. However, only three crosslinked species were observed, as opposed to the six species expected if any of the six UvsY subunits could be simultaneously crosslinked to dT_{24}. By comparing with standards, the molecular weight of the three crosslinked species appear to correspond to a dT_{24} molecule covalently linked to 1, 3 and 5–6 UvsY monomers, respectively. Control experiments with dT_{24} alone resulted in no crosslinking, therefore all crosslinked species were generated by protein–ssDNA crosslinking (Figure 6, lanes 3 and 5). Other control experiments with UvsY protein alone (detected by silver staining; data not shown) contained a small amount of crosslinked, dimeric UvsY, which has an electrophoretic mobility distinct from all of the protein–DNA crosslinked species visible in Figure 6. The data suggest that there is asymmetry regarding how individual subunits interact with a long ssDNA molecule that transits the entire UvsY hexamer. This asymmetry may be an intrinsic property of the UvsY hexamer (see below), or it may be imposed on the hexamer by the chain topology of ssDNA.

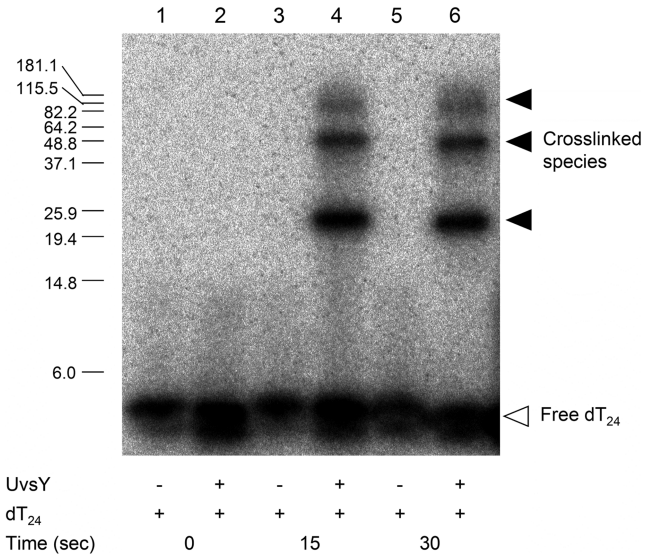

Figure 6. Photochemical crosslinking of UvsY–dT_{24} complex. UvsY was crosslinked to 5′-[^{32}P]-labeled dT_{24} by 254 nm UV exposure as described in 'Materials and Methods' section. The crosslinked species (black arrows) were separated from free 5′-[^{32}P]-labeled dT_{24} (white arrow) by SDS–PAGE and visualized by autoradiography. Different exposure times (0, 15 and 30 s) were applied as indicated and pre-stained molecular weight standards (left) were used to estimate the molecular weight of the crosslinked species.

Hydrodynamic modeling suggests a ring-like arrangement of UvsY subunits

Sedimentation velocity data were used to estimate the overall apparent shape of the UvsY hexamer and of the hexamer–ssDNA complex from f/f_0, the hydrodynamic frictional ratio. Experimental frictional coefficients (f-values) for $UvsY_6$ and $UvsY_6$–ssDNA were calculated from published $s^0_{20,w}$ values (22), and are listed in Table 3. When compared with the theoretical frictional coefficient, f_0, calculated for a rigid, incompressible sphere of identical molecular mass and partial specific volume, it appears that the overall shape of UvsY deviates markedly from a spheroid, as $f/f_0 = 1.2$ for both $UvsY_6$ and $UvsY_6$–dT_{25} complexes. It is not possible to model UvsY oligomeric shapes directly from the sedimentation properties of

Table 3. Hydrodynamic parameters of $UvsY_6$ hexamers in the presence and absence of dT_{25} oligonucleotide

	M_r[a] (Da)	$\bar{v}$[b] (cm^3/g)	$s^0_{20,w}$[c] ($\times 10^{-13}$ s)	f[d] ($\times 10^{-8}$ g/s)	f_0[e] ($\times 10^{-8}$ g/s)	f/f_0[f]
$UvsY_6$	94 389	0.738	6.0	6.9	5.8	1.2
$UvsY_6$–dT_{25}	101 910	0.723	6.5	7.3	5.9	1.2

[a]Molecular weight, calculated from sequence.
[b]Partial specific volume. $\bar{v}$ for $UvsY_6$ was calculated from the amino acid sequence. $\bar{v}$ for $UvsY_6$–dT_{25} is the weight average assuming $\bar{v} = 0.55$ cm^3/g for dT_{25}. See 'Materials and Methods' section.
[c]Sedimentation coefficient at 20°C in water, corrected to zero concentration of the sedimenting solute. Data adapted from ref. (22).
[d]Frictional coefficient, calculated from empirical $s^0_{20,w}$ values using Equation (3).
[e]Theoretical frictional coefficient for a rigid, incompressible sphere of identical mass and partial specific volume as the sedimenting solute. Calculated as described in 'Materials and Methods' section.
[f]Frictional ratio.

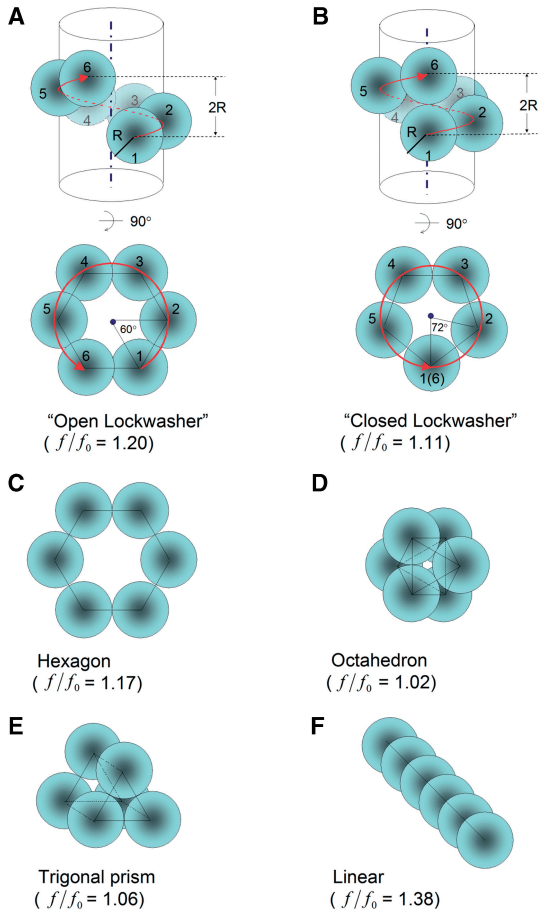

Figure 7. Hydrodynamic modeling of hexameric assemblies of spherical beads. The frictional ratio f/f_0 was calculated for modeled assemblies as described in 'Materials and Methods' and 'Result' sections. Assemblies are assumed to be rigid, and composed of identical rigid, incompressible spheres. R is the equivalent radius of each sphere. The UvsY hexamer (f/f_0 = 1.2) shows similarity to the open lockwasher (**A**) and hexagonal (**C**) models.

monomers, because dissociation of UvsY hexamers into monomers requires chaotropic reagents (22). Therefore we estimated the oligomeric shape of UvsY indirectly by comparing the experimental f/f_0 values to those of theoretical oligomers (36–40). Figure 7 presents a series of theoretical models and the corresponding frictional ratios for hexameric associations of UvsY monomers based on this method. The method assumes that each UvsY subunit is globular and approximately spherical in shape. Based on this assumption, the observed frictional ratio of $UvsY_6 \pm dT_{25}$ (f/f_0 = 1.2) is best approximated by ring-like structures such as the hexagonal model in Figure 7C (f/f_0 = 1.17) or the open lockwasher model in Figure 7A (f/f_0 = 1.20). Other reasonable hexameric arrangements shown in Figure 7 are not consistent with the experimental data. Independent biochemical evidence exists for structural asymmetry within the UvsY hexamer: UvsY contains one cysteine residue per monomer (Cys-110) (35) and therefore six per hexamer. However, covalent labeling of Cys-110 with excess 6-iodoacetamidofluorescein (6-IAF) under native hexamer conditions reproducibly yields a stoichiometry of one fluorescein moiety incorporated per hexamer (J. Liu, H. Xu and S. Morrical, unpublished results), suggesting that Cys-110 is only accessible to reagent at one end of an asymmetric structure. This finding is consistent either with a stable open lockwasher arrangement or with an equilibrium between open and closed forms of the hexagonal ring.

DISCUSSION

ssDNA wrapping promotes high-affinity binding by UvsY

The data demonstrate that UvsY has a strong thermodynamic preference for binding to relaxed ssDNA over relaxed dsDNA lattices (Figure 1, Table 1). The affinity differential is a result of ssDNA wrapping by UvsY. Results demonstrate that ssDNA is wrapped around hexamers of UvsY protein, since ssDNA contacts multiple subunits within each hexamer under monodisperse conditions (Figures 5 and 6) (22). The hydrodynamic and biochemical properties of UvsY hexamers are consistent with a ring- or lockwasher-like arrangement of subunits (Table 3; Figure 7A and C), suggesting that UvsY may wrap ssDNA into ring- or screw-like structures.

DNA stretching studies provide additional evidence for ssDNA wrapping by UvsY at the single-molecule level (24). Force spectroscopy measurements indicate that UvsY strongly wraps ssDNA that is created by the exposure of stretched dsDNA molecules to glyoxal. Presumably UvsY cannot wrap dsDNA because its persistence length is much higher than that of ssDNA (45). ssDNA wrapping occurs at low stretching forces where the DNA is relatively relaxed, whereas wrapping is suppressed when the DNA is under tension. This suppression of wrapping leads to the loss of preferential binding to ssDNA under the conditions of the DNA stretching experiments—in fact, UvsY binds tighter to dsDNA than to ssDNA under high stretching forces (24). In contrast, under relaxed conditions where ssDNA wrapping occurs, UvsY exhibits ~1000-fold higher affinity for ssDNA than for dsDNA (Figure 1, Table 1). Further evidence that ssDNA wrapping promotes high-affinity UvsY–ssDNA binding comes from the observation that a monomeric form of UvsY exhibits a 10^4-fold reduced affinity for ssDNA while retaining the same binding site size (4 nt residues per monomer) on ssDNA that is observed in hexameric UvsY (46).

Electrostatics of UvsY–DNA interactions

Results indicate that UvsY uses different electrostatic binding modes for ssDNA and dsDNA, based on the large difference in the magnitude of the salt effect on K_{ss} versus K_{ds} (Figure 4, Table 2). Theoretically the magnitude of the salt effect on the affinity parameter for a protein–DNA interaction is defined as

$$d\log K/d\log[NaCl] = -m'\psi - a \quad (7)$$

where m' equals the number of contacts between negatively charged DNA phosphate residues and positively

charged protein amino acid residues, a is the number of anions displaced from the protein upon binding to DNA, and Ψ is a partitioning constant equal to 0.71 for ssDNA or 0.88 for dsDNA (41–44). In this study, we used the quantitative ssDNA–cellulose method to measure UvsY interactions with isolated sites on native ssDNA, and found a large salt effect on K_{ss} ($d\log K_{ss}/d\log[NaCl] = -13.9$). Previously we studied UvsY–ssDNA interactions by titrating etheno-modified ssDNA (εDNA) with protein at different salt concentrations, and found a much smaller salt effect ($d\log K_{ss}/d\log[NaCl] = -6.8$) (23). The latter value is similar to the salt effect on dsDNA binding ($d\log K_{ds}/d\log[NaCl] = -6.6$) determined from dsDNA–cellulose binding data in this study (Figure 4, Table 2). Possible explanations for the method-dependent difference in salt effects on UvsY–ssDNA interactions include:

Effects of DNA persistence length. The etheno modification could increase the persistence length of ssDNA, making it difficult to be fully wrapped by UvsY hexamers, as is the case for dsDNA. This could explain the nearly identical salt effects on UvsY–εDNA (23) and UvsY–dsDNA interactions (Figure 4, Table 2).

Effects of protein–ssDNA-binding density. An alternative explanation is that binding density could affect the degree of ssDNA wrapping by UvsY hexamers. Quantitative ssDNA–cellulose binding experiments are carried out at very low binding density ($\nu \leq 3 \times 10^{-4}$ UvsY hexamers per nucleotide residue), so that K_{ss} values are for individual hexamers interacting with isolated sites on ssDNA. In contrast, using the εDNA titration method, K_{ss} values are determined from the midpoints of titration curves where $\nu = 0.5$ meaning that the lattice is relatively crowded with protein. The larger salt effect on K_{ss} seen at low binding density on relaxed ssDNA may represent a fully wrapped $UvsY_6$–ssDNA complex. Full wrapping might be precluded at high binding density, however. Such is the case with *Escherichia coli* SSB protein, which binds ssDNA in the fully-wrapped SSB_{65} mode at low binding density and in the partially-wrapped SSB_{33} mode at high binding density (47). Thus high binding density might force UvsY to bind to ssDNA in a partially wrapped or unwrapped mode that resembles the UvsY–dsDNA complex. This could also explain the nearly identical salt effects observed in UvsY–εDNA titrations (23) and in UvsY–dsDNA binding studies (Figure 4, Table 2).

Role of Lys-58 and Arg-60 residues in UvsY–DNA interactions

The K58A and R60A mutations neutralize basic residues within a conserved LKARLDY motif found in the N-terminal domain of UvsY that is important for DNA binding (18,27). The motif is conserved in several other DNA-binding proteins including human ERCC2 and yeast Rad3 proteins (48). By attenuating potential electrostatic contacts with DNA, the single mutant $UvsY_{K58A}$ is expected to have lower affinity compared to wild-type and the affinity of double mutant $UvsY_{K58A,\ R60A}$ should be even lower. This is exactly what is observed in this study. The magnitude of the salt-dependence of K_{ss} observed for $UvsY_{R58A}$–ssDNA interactions is also lower than wild-type ($d\log K_{ss}/d\log[NaCl] = -1.7$ versus -13.9, respectively), consistent with a loss of electrostatic protein–DNA contacts. The large magnitude of this change is surprising considering the single amino acid change, however, and indicates that the K58A (and presumably R60A) mutations compromise a larger electrostatic network involved in UvsY–DNA contacts and/or in the wrapping of ssDNA around UvsY hexamers.

A mechanism for lattice selectivity during T4 recombination

The results of this study suggest that UvsY could play an important role in the selective assembly of presynaptic filaments on ssDNA in the presence of excess dsDNA, a partitioning that is essential for recombination transactions both *in vivo* and *in vitro*. Driving this partitioning is the >1000-fold intrinsic affinity advantage of UvsY–ssDNA over UvsY–dsDNA interactions at physiologically relevant ionic strengths (Table 1). Like many recombinases of the RecA/Rad51 family, the T4 UvsX protein binds strongly to dsDNA as well as to ssDNA (8,49) (R. Maher and S. Morrical, manuscript in preparation). In the case of eukaryotic Rad51, pre-bound dsDNA inhibits DNA strand exchange, thus the translocation/remodeling activities of Rad54 protein are needed to disrupt inappropriate Rad51–dsDNA contacts and to promote productive filament assembly on ssDNA (50). In the T4 recombination system, the need for a Rad54-like function may be circumvented by UvsY, which by virtue of its strong affinity preference for ssDNA may selectively recruit UvsX to and nucleate filament formation on ssDNA. Reinforcing this partitioning is the fact that UvsY and nucleoside triphosphate increase UvsX–ssDNA binding affinity synergistically (18). The combination of factors would therefore result in stringent discrimination in favor of presynaptic filament assembly on ssDNA.

A double hand-off mechanism for presynaptic filament assembly

The ability of UvsY to bind to ssDNA in either extended or wrapped conformations has important implications for its recombination mediator functions. As a classical recombination mediator protein, UvsY promotes the loading of UvsX recombinase onto pre-existing Gp32–ssDNA complexes to form presynaptic filaments with concomitant displacement of Gp32 from ssDNA. Ensemble, single-molecule and mutagenesis data are consistent with a model in which UvsY induces changes in ssDNA structure that destabilize Gp32–ssDNA interactions and stabilize UvsX–ssDNA interactions (17,18,24,25). Previous studies of the $UvsY_{K58A}$ and $UvsY_{K58A,R60A}$ mutants, which bind weakly to ssDNA, established that UvsY–ssDNA interactions are the major factor controlling UvsY stabilization of UvsX–ssDNA interactions, while UvsY–UvsX protein–protein interactions play a minor role in stabilizing UvsX–ssDNA interactions (18,27).

Many nucleic acid pathways channel their DNA or RNA substrates through a series of hand-off transactions in which a nucleic acid intermediate is passed directly from

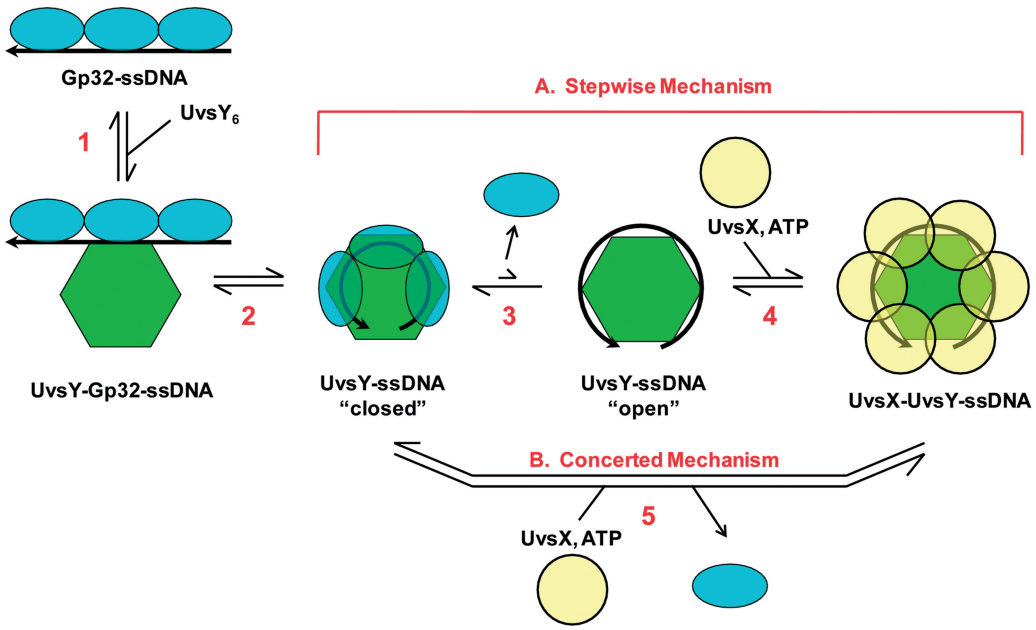

Figure 8. A double hand-off model for the mechanism of mediator protein UvsY in T4 presynaptic filament assembly. Adapted with modifications from ref. (25). UvsY protein facilitates the loading of UvsX recombinase onto ssDNA and the concomitant displacement of Gp32 ssDNA-binding protein from ssDNA. The figure shows UvsX loading and Gp32 displacement from the perspective of a single UvsY hexamer, as if looking down the helical axis of a nascent presynaptic filament. The cooperative binding of Gp32 to ssDNA extends the polynucleotide lattice. The first hand-off occurs as hexameric UvsY recognizes and binds to the extended ssDNA (step 1), then converts it into a wrapped conformation(s) (steps 2 and 3), destabilizing Gp32–ssDNA interactions in the process. The UvsY-wrapped ssDNA complex is postulated to be in equilibrium between 'closed' and 'open' conformations (step 3), the latter of which is recognized by the ATP-bound form of UvsX protein to nucleate presynaptic filament assembly (step 4) while displacing Gp32. (**A**) Steps 3 and 4 constitute a step-wise mechanism for Gp32 displacement and UvsX loading by UvsY, which may occur under low-salt conditions. (**B**) Under high-salt conditions UvsY does not displace Gp32 from ssDNA directly, so filament assembly likely occurs by a concerted mechanism in which synergistic action of UvsY and ATP-bound UvsX is required to displace Gp32. See text for details.

one protein in the pathway to the next without ever being released as free nucleic acid (51–54). The advantages of this strategy include: potential cytotoxic effects of the nucleic acid intermediate are minimized by keeping it sequestered; also the nucleic acid is protected from inappropriate degradation or side reactions. Evidence suggests that ssDNA in recombination pathways is similarly channeled (25). Based on the DNA-binding properties of the three protein players, we propose that the loading of UvsX recombinase onto Gp32–ssDNA complexes proceeds through a series of at least two sequential hand-off steps (Figure 8) (12,24,25): Gp32 first binds to ssDNA and converts it into an extended form resembling the mechanically stretched DNA that was sampled in single-molecule experiments. The first hand-off occurs as UvsY recognizes and binds to the extended ssDNA, then converts it into a wrapped form that destabilizes Gp32–ssDNA interactions. The UvsY-wrapped ssDNA complex is postulated to be in equilibrium between 'closed' and 'open' states (25). The closed form is the one that destabilizes Gp32–ssDNA interactions, and it is inaccessible to UvsX. The open form is optimal for UvsX–ssDNA interactions. The second hand-off occurs as the ATP-bound form of UvsX recognizes and binds to the open UvsY–ssDNA structure, nucleating or propagating a UvsX–ssDNA filament while inducing Gp32 to leave. Conceivably UvsX loading/Gp32 displacement could occur either in a stepwise fashion (Figure 8A) or in a concerted fashion (Figure 8B) depending on solution variables including salt concentration (24,25). Superimposed on the underlying hand-off mechanism are effects involving UvsX cooperativity (55) and a nucleotide exchange factor activity of UvsY (25) that have not been fully explored. Also, linking ATP hydrolysis by UvsX to the hand-off scheme creates dynamic instability in presynaptic filaments that may be linked to filament turnover, translocation, or DNA strand exchange activity (12,13).

Implications for other recombination mediator proteins

Previously, recombination mediator proteins have been thought of primarily as factors that facilitate the exchange of bound SSB proteins for recombinase on ssDNA (10). Results of this study suggest an additional function for RMPs: that of recruiting recombinases onto ssDNA while minimizing inappropriate recombinase–dsDNA interactions during the presynaptic phase of homologous recombination. The universal role of RMPs in promoting recombinase–ssDNA assembly suggests that different RMPs may share common mechanistic features. It is noteworthy that, like UvsY, many other well-characterized RMPs have oligomeric structures with multiple ssDNA-binding sites. Bacterial RMPs include the RecO and RecR proteins which function together as hetero-oligomers (56,57). The RecR protein of *Deinococcus radiodurans* crystallizes as a tetrameric ring, exhibits both ssDNA- and dsDNA-binding activity, and interacts with RecO, whereas RecO itself contains multiple DNA-binding sites (58,59). Eukaryotic RMPs include

the Rad52 proteins, the human ortholog of which appears to function as a heptameric ring, and ssDNA is proposed to wind around the ring structure (60–62). Therefore organizing ssDNA by wrapping may be a common element of the function of certain homo- or hetero-oligomeric RMPs.

Other eukaryotic proteins with RMP activity include Rad51 paralogs and the tumor suppressor gene product Brca2 (63). Rad51 paralogs (Rad55, Rad57 in *Saccharomyces cerevisiae*; Rad51B, Rad51C, Rad51D, Xrcc2, Xrcc3 in humans) exist as heterodimers or oligomers (64,65). Subsets of the human Rad51 paralogs exist in two different ring-shaped complexes, BCDX2 and CX3, and bind strongly to Holliday junctions (66). Other aspects of their DNA-binding activities are incompletely understood. Brca2 is thought to function as a monomer; nevertheless it contains three OB fold motifs that bind ssDNA, as well as sites for structure-specific DNA binding (67). So it remains a possibility that Brca2, in addition to its well-characterized protein-protein interactions with Rad51 (68), also promotes recombination through changes in ssDNA structure.

ACKNOWLEDGEMENTS

The authors thank Jennifer Tomczak for technical assistance and Dr Jill Bleuit for purification of two UvsY mutant proteins.

FUNDING

National Institute of General Medical Sciences, NIH, HHS, USA (grant number R01 GM48847). Funding for open access charge: National Institutes of Health (grant number R01 GM48847).

Conflict of interest statement. None declared.

REFERENCES

1. Kowalczykowski,S.C., Dixon,D.A., Eggleston,A.K., Lauder,S.D. and Rehrauer,W.M. (1994) Biochemistry of homologous recombination in Escherichia coli. *Microbiol. Rev.*, **58**, 401–465.
2. Symington,L.S. (2002) Role of RAD52 epistasis group genes in homologous recombination and double-strand break repair. *Microbiol. Mol. Biol. Rev.*, **66**, 630–670, table of contents.
3. Bianco,P.R., Tracy,R.B. and Kowalczykowski,S.C. (1998) DNA strand exchange proteins: a biochemical and physical comparison. *Front Biosci.*, **3**, D570–D603.
4. Sung,P., Trujillo,K.M. and Van Komen,S. (2000) Recombination factors of Saccharomyces cerevisiae. *Mutat. Res.*, **451**, 257–275.
5. Jasin,M. (2002) Homologous repair of DNA damage and tumorigenesis: the BRCA connection. *Oncogene*, **21**, 8981–8993.
6. Scully,R. (2000) Role of BRCA gene dysfunction in breast and ovarian cancer predisposition. *Breast Cancer Res.*, **2**, 324–330.
7. Sung,P. and Robberson,D.L. (1995) DNA strand exchange mediated by a RAD51-ssDNA nucleoprotein filament with polarity opposite to that of RecA. *Cell*, **82**, 453–461.
8. Namsaraev,E.A. and Berg,P. (1998) Binding of Rad51p to DNA. Interaction of Rad51p with single- and double-stranded DNA. *J. Biol. Chem.*, **273**, 6177–6182.
9. Baumann,P. and West,S.C. (1997) The human Rad51 protein: polarity of strand transfer and stimulation by hRP-A. *EMBO J.*, **16**, 5198–5206.
10. Beernink,H.T. and Morrical,S.W. (1999) RMPs: recombination/replication mediator proteins. *Trends Biochem. Sci.*, **24**, 385–389.
11. Bleuit,J.S., Xu,H., Ma,Y., Wang,T., Liu,J. and Morrical,S.W. (2001) Mediator proteins orchestrate enzyme-ssDNA assembly during T4 recombination-dependent DNA replication and repair. *Proc. Natl Acad. Sci. USA*, **98**, 8298–8305.
12. Liu,J. and Morrical,S.W. (2010) Dynamics of protein-ssDNA interactions in the bacteriophage T4 homologous recombination system. In Williams,M.C. and Maher,L.J. (eds), *Biophysics of DNA-Protein Interactions: From Single Molecules to Biological Systems*. Springer, NY, in press.
13. Liu,J., Qian,N. and Morrical,S.W. (2006) Dynamics of bacteriophage T4 presynaptic filament assembly from extrinsic fluorescence measurements of Gp32-single-stranded DNA interactions. *J. Biol. Chem.*, **281**, 26308–26319.
14. Yonesaki,T. and Minagawa,T. (1989) Synergistic action of three recombination gene products of bacteriophage T4, uvsX, uvsY, and gene 32 proteins. *J. Biol. Chem.*, **264**, 7814–7820.
15. Harris,L.D. and Griffith,J.D. (1989) UvsY protein of bacteriophage T4 is an accessory protein for in vitro catalysis of strand exchange. *J. Mol. Biol.*, **206**, 19–27.
16. Kodadek,T., Gan,D.C. and Stemke-Hale,K. (1989) The phage T4 uvs Y recombination protein stabilizes presynaptic filaments. *J. Biol. Chem.*, **264**, 16451–16457.
17. Sweezy,M.A. and Morrical,S.W. (1999) Biochemical interactions within a ternary complex of the bacteriophage T4 recombination proteins uvsY and gp32 bound to single-stranded DNA. *Biochemistry*, **38**, 936–944.
18. Liu,J., Bond,J.P. and Morrical,S.W. (2006) Mechanism of presynaptic filament stabilization by the bacteriophage T4 UvsY recombination mediator protein. *Biochemistry*, **45**, 5493–5502.
19. Boyle,J.M. and Symonds,N. (1969) Radiation-sensitive mutants of T4D. I. T4y: a new radiation-sensitive mutant; effect of the mutation on radiation survival, growth and recombination. *Mutat. Res*, **8**, 431–439.
20. Cunningham,R.P. and Berger,H. (1977) Mutations affecting genetic recombination in bacteriophage T4D. I. Pathway analysis. *Virology*, **80**, 67–82.
21. Melamede,R.J. and Wallace,S.S. (1977) Properties of the nonlethal recombinational repair x and y mutants of bacteriophage T4. II. DNA synthesis. *J. Virol.*, **24**, 28–40.
22. Beernink,H.T. and Morrical,S.W. (1998) The uvsY recombination protein of bacteriophage T4 forms hexamers in the presence and absence of single-stranded DNA. *Biochemistry*, **37**, 5673–5681.
23. Sweezy,M.A. and Morrical,S.W. (1997) Single-stranded DNA binding properties of the uvsY recombination protein of bacteriophage T4. *J. Mol. Biol.*, **266**, 927–938.
24. Pant,K., Shokri,L., Karpel,R.L., Morrical,S.W. and Williams,M.C. (2008) Modulation of T4 gene 32 protein DNA binding activity by the recombination mediator protein UvsY. *J. Mol. Biol.*, **380**, 799–811.
25. Farb,J.N. and Morrical,S.W. (2009) Functional complementation of UvsX and UvsY mutations in the mediation of T4 homologous recombination. *Nucleic Acids Res.*, **37**, 2336–2345.
26. Alberts,B.M. and Herrick,G. (1971) DNA-cellulose chromatography. *Methods in Enzymol.*, **22**, 198–217.
27. Bleuit,J.S., Ma,Y., Munro,J. and Morrical,S.W. (2004) Mutations in a conserved motif inhibit single-stranded DNA binding and recombination mediator activities of bacteriophage T4 UvsY protein. *J. Biol. Chem.*, **279**, 6077–6086.
28. Morrical,S.W., Hempstead,K. and Morrical,M.D. (1994) The gene 59 protein of bacteriophage T4 modulates the intrinsic and single-stranded DNA-stimulated ATPase activities of gene 41 protein, the T4 replicative DNA helicase. *J. Biol. Chem.*, **269**, 33069–33081.
29. Gill,S.C. and von Hippel,P.H. (1989) Calculation of protein extinction coefficients from amino acid sequence data. *Anal. Biochem.*, **182**, 319–326.
30. deHaseth,P.L., Gross,C.A., Burgess,R.R. and Record,M.T. Jr (1977) Measurement of binding constants for protein-DNA interactions by DNA-cellulose chromatography. *Biochemistry*, **16**, 4777–4783.

31. Kowalczykowski,S.C., Paul,L.S., Lonberg,N., Newport,J.W., McSwiggen,J.A. and von Hippel,P.H. (1986) Cooperative and noncooperative binding of protein ligands to nucleic acid lattices: experimental approaches to the determination of thermodynamic parameters. *Biochemistry*, **25**, 1226–1240.
32. Ames,B.N. (1966) Assay of inorganic phosphate, total phosphates and phosphatases. *Methods in Enzymol.*, **8**, 115–118.
33. Yphantis,D.A. (1964) Equilibrium ultracentrifugation of dilute solutions. *Biochemistry*, **47**, 297–317.
34. Laue,T.M., Shah,B.D., Ridgeway,T.M. and Pelletier,S.L. (1992) Computer-aided interpretation of analytical sedimentation data for proteins. In Harding,S.E., Rowe,A.J. and Horton,J.C. (eds), *Analytical Ultracentrifugation in Biochemistry and Polymer Science*. Royal Society of Chemistry, Cambridge, pp. 90–125.
35. Gruidl,M.E. and Mosig,G. (1986) Sequence and transcripts of the bacteriophage T4 DNA repair gene uvsY. *Genetics*, **114**, 1061–1079.
36. Teller,D.C. (1976) Accessible area, packing volumes and interaction surfaces of globular proteins. *Nature*, **260**, 729–731.
37. Bloomfield,V., Dalton,W.O. and Van Holde,K.E. (1967) Frictional coefficients of multisubunit structures. I. Theory. *Biopolymers*, **5**, 135–148.
38. Bloomfield,V., Van Holde,K.E. and Dalton,W.O. (1967) Frictional coefficients of multisubunit structures. II. Application to proteins and viruses. *Biopolymers*, **5**, 149–159.
39. Kirkwood,J.G. (1954) The general theory of irreversible processes in solutions of macromolecules. *J. Polymer Sci.*, **12**, 1–14.
40. de la Torre,J.C. (1992) Sedimentation coefficients of complex biological particles. In Harding,S.E., Rowe,A.J. and Horton,J.C. (eds), *Analytical Ultracentrifugation in Biochemistry and Polymer Science*. Royal Society of Chemistry, Cambridge, pp. 333–345.
41. Record,M.T. Jr, deHaseth,P.L. and Lohman,T.M. (1977) Interpretation of monovalent and divalent cation effects on the lac repressor-operator interaction. *Biochemistry*, **16**, 4791–4796.
42. Menetski,J.P. and Kowalczykowski,S.C. (1985) Interaction of recA protein with single-stranded DNA. Quantitative aspects of binding affinity modulation by nucleotide cofactors. *J. Mol. Biol.*, **181**, 281–295.
43. Record,M.T. Jr, Lohman,M.L. and De Haseth,P. (1976) Ion effects on ligand-nucleic acid interactions. *J. Mol. Biol.*, **107**, 145–158.
44. deHaseth,P.L., Lohman,T.M. and Record,M.T. Jr (1977) Nonspecific interaction of lac repressor with DNA: an association reaction driven by counterion release. *Biochemistry*, **16**, 4783–4790.
45. Williams,M.C. and Rouzina,I. (2002) Force spectroscopy of single DNA and RNA molecules. *Curr. Opin. Struct. Biol.*, **12**, 330–336.
46. Ando,R.A. and Morrical,S.W. (1999) Relationship between hexamerization and ssDNA binding affinity in the uvsY recombination protein of bacteriophage T4. *Biochemistry*, **38**, 16589–16598.
47. Lohman,T.M. and Overman,L.B. (1986) Two binding modes in Escherichia coli single strand binding protein-single stranded DNA complexes: modulation by NaCl concentration. *J. Biol. Chem.*, **260**, 3594–3603.
48. Weber,C.A., Salazar,E.P., Stewart,S.A. and Thompson,L.H. (1990) ERCC2: cDNA cloning and molecular characterization of a human nucleotide excision repair gene with high homology to yeast RAD3. *Embo J.*, **9**, 1437–1447.
49. Zaitseva,E.M., Zaitsev,E.N. and Kowalczykowski,S.C. (1999) The DNA binding properties of Saccharomyces cerevisiae Rad51 protein. *J. Biol. Chem.*, **274**, 2907–2915.
50. Solinger,J.A., Kiianitsa,K. and Heyer,W.D. (2002) Rad54, a Swi2/Snf2-like recombinational repair protein, disassembles Rad51:dsDNA filaments. *Mol. Cell*, **10**, 1175–1188.
51. Echols,H. (1986) Multiple DNA-protein interactions governing high-precision DNA transactions. *Science*, **233**, 1050–1056.
52. Lopper,M., Boonsombat,R., Sandler,S.J. and Keck,J.L. (2007) A hand-off mechanism for primosome assembly in replication restart. *Mol. Cell*, **26**, 781–793.
53. Liu,Y., Prasad,R., Beard,W.A., Kedar,P.S., Hou,E.W., Shock,D.D. and Wilson,S.H. (2007) Coordination of steps in single-nucleotide base excision repair mediated by apurinic/apyrimidinic endonuclease 1 and DNA polymerase beta. *J. Biol. Chem.*, **282**, 13532–13541.
54. Hitomi,K., Iwai,S. and Tainer,J.A. (2007) The intricate structural chemistry of base excision repair machinery: implications for DNA damage recognition, removal, and repair. *DNA Repair*, **6**, 410–428.
55. Ando,R.A. and Morrical,S.W. (1998) Single-stranded DNA binding properties of the UvsX recombinase of bacteriophage T4: binding parameters and effects of nucleotides. *J. Mol. Biol.*, **283**, 785–796.
56. Umezu,K., Chi,N.W. and Kolodner,R.D. (1993) Biochemical interaction of the Escherichia coli RecF, RecO, and RecR proteins with RecA protein and single-stranded DNA binding protein. *Proc. Natl Acad. Sci. USA*, **90**, 3875–3879.
57. Umezu,K. and Kolodner,R.D. (1994) Protein interactions in genetic recombination in Escherichia coli. Interactions involving RecO and RecR overcome the inhibition of RecA by single-stranded DNA-binding protein. *J. Biol. Chem.*, **269**, 30005–30013.
58. Leiros,I., Timmins,J., Hall,D.R. and McSweeney,S. (2005) Crystal structure and DNA-binding analysis of RecO from Deinococcus radiodurans. *Embo J.*, **24**, 906–918.
59. Lee,B.I., Kim,K.H., Park,S.J., Eom,S.H., Song,H.K. and Suh,S.W. (2004) Ring-shaped architecture of RecR: implications for its role in homologous recombinational DNA repair. *EMBO J.*, **23**, 2029–2038.
60. Stasiak,A.Z., Larquet,E., Stasiak,A., Muller,S., Engel,A., Van Dyck,E., West,S.C. and Egelman,E.H. (2000) The human Rad52 protein exists as a heptameric ring. *Curr. Biol.*, **10**, 337–340.
61. Kagawa,W., Kurumizaka,H., Ishitani,R., Fukai,S., Nureki,O., Shibata,T. and Yokoyama,S. (2002) Crystal structure of the homologous-pairing domain from the human Rad52 recombinase in the undecameric form. *Mol. Cell*, **10**, 359–371.
62. Singleton,M.R., Wentzell,L.M., Liu,Y., West,S.C. and Wigley,D.B. (2002) Structure of the single-strand annealing domain of human RAD52 protein. *Proc. Natl Acad. Sci. USA*, **99**, 13492–13497.
63. San Filippo,J., Sung,P. and Klein,H. (2008) Mechanism of eukaryotic homologous recombination. *Annu. Rev. Biochem.*, **77**, 229–257.
64. Sung,P. (1997) Yeast Rad55 and Rad57 proteins form a heterodimer that functions with replication protein A to promote DNA strand exchange by Rad51 recombinase. *Genes Dev.*, **11**, 1111–1121.
65. Masson,J.Y., Tarsounas,M.C., Stasiak,A.Z., Stasiak,A., Shah,R., McIlwraith,M.J., Benson,F.E. and West,S.C. (2001) Identification and purification of two distinct complexes containing the five RAD51 paralogs. *Genes Dev.*, **15**, 3296–3307.
66. Compton,S.A., Ozgur,S. and Griffith,J.D. (2010) Ring-shaped Rad51 paralog protein complexes bind holliday junctions and replication forks as visualized by electron micrsocopy. *J. Biol. Chem*, [March 5; Epub ahead of print].
67. Yang,H., Jeffrey,P.D., Miller,J., Kinnucan,E., Sun,Y., Thoma,N.H., Zheng,N., Chen,P.L., Lee,W.H. and Pavletich,N.P. (2002) BRCA2 function in DNA binding and recombination from a BRCA2-DSS1-ssDNA structure. *Science*, **297**, 1837–1848.
68. Pellegrini,L., Yu,D.S., Lo,T., Anand,S., Lee,M., Blundell,T.L. and Venkitaraman,A.R. (2002) Insights into DNA recombination from the structure of a RAD51-BRCA2 complex. *Nature*, **420**, 287–293.